Inorganic Chemistry
Article

*Inorg. Chem.* **2010**, *49*, 7257–7265 **7257**
DOI: 10.1021/ic901261u

# Polymorphic Crystal Approach to Changing the Emission of $[AuCl(PPh_3)_2]$, Analyzed by Direct Observation of the Photoexcited Structures by X-ray Photocrystallography

**Manabu Hoshino,[†] Hidehiro Uekusa,*[,†] Satoshi Ishii,[‡] Takuhiro Otsuka,[‡] Youkoh Kaizu,[†,‡] Yoshiki, Ozawa,[§] and Koshiro Toriumi[§]**

[†]*Department of Chemistry and Materials Science, and* [‡]*Department of Chemistry, Tokyo Institute of Technology, 2-12-1, Ookayama, Meguro-ku, Tokyo, 152-8551, Japan , and* [§]*Department of Materials Science, University of Hyogo, 3-2-1, Kouto, Kamigori-cho, Ako-gun, Hyogo, 678-1297, Japan*

Received July 1, 2009

The photoexcited charge-transferred state of $[AuCl(PPh_3)_2]$ in a novel polymorphic crystal form was directly observed by X-ray photocrystallographic analysis. Its photoexcited state was completely different from the one generated in the known crystal of $[AuCl(PPh_3)_2]$; the photoexcited bond-shrunk state was generated in the known crystal. This difference in the generated photoexcited state was clearly reflected by the difference in emission color. While the known crystal form showed green phosphorescence, the novel form showed blue phosphorescence under UV irradiation. The difference in the generated photoexcited state was due to the differences in steric hindrance in the crystal; bond shortening by photoexcitation was sterically allowed in the known form, while on the other hand, it was restricted in the novel form. Therefore, instead of the bond-shrunk state, the charge-transferred excited state became the lowest triplet state, and the emission color changed from green to blue (i.e., a blue shift of the emission wavelength was observed). These results mean that the photoexcited structure and the emission color of $[AuCl(PPh_3)_2]$ can be controlled by designing the molecular environment in the crystal.

## Introduction

Monovalent gold (Au(I)) complexes are known to display visible phosphorescence under UV irradiation.[1−3] Their emission quantum efficiencies are relatively high, and these emissions are observed even at room temperature.[4−6] These emission characteristics make these complexes suitable for use as electroluminescent (EL) materials.[7] Therefore, to develop novel EL materials by utilizing these complexes, a great deal of research has been undertaken to understand and control these emissions. For example, emissions from $[Au(R_2\text{-bimy})L]$ (R = Et, Me; bimy = benzimidazol-2-ylidene; L = Cl, Br, I, thiophenolate, phenylacetylide) and [Au(TPA)R] (TPA = 1,3,5-triaza-7-phosphaadamantanetriylphsphine; R = *o*-methylthiophenolate, *m*-chlorothiophenolate, *p*-chlorothiophenolate) originate in the radiative deactivation from a ligand-related excited state, such as a photoexcited intraligand (IL) or ligand-to-metal charge-transfer (LMCT) state. On the basis of this understanding, the emission colors of these complexes were tuned by synthesizing derivative complexes with different ligands.[8,9]

In the case of Au(I) complexes in which linear two-coordinated Au(I) centers are arranged within the sum of the van der Waals radii (∼3.6 Å), the weak interaction among Au(I) centers (the aurophilic interaction) was closely related to the emission properties of these complexes.[10,11] The relationship between the strengths (or distance) of the aurophilic interactions and the emission color has been studied using spectroscopic and crystallographic analyses.[12,13] This relationship led to several emission tuning techniques which changed the distance of the aurophilic interactions. For example, Ito et al. reported the mechanochromism of $[(C_6F_5Au)_2(\mu\text{-}1,4\text{-diisocyanobenzene})]$; its emission color was altered from blue to

*To whom correspondence should be addressed. E-mail: uekusa@cms.titech.ac.jp.

(1) Yam, V. W.-W.; Cheng, E. C.-C. *Chem. Soc. Rev.* **2008**, *37*, 1806–1813.
(2) Vogler, A.; Kunkely, H. *Coord. Chem. Rev.* **2001**, *219*−*221*, 489–507.
(3) Yam, V. W.-W.; Lo, K. K.-W. *Chem. Soc. Rev.* **1999**, *28*, 323–334.
(4) King, C.; Khan, M. N. I.; Staples, R. J.; Fackler, J. J. P. *Inorg. Chem.* **1992**, *31*, 3236–3238.
(5) McCleskey, T. M.; Gray, H. B. *Inorg. Chem.* **1992**, *31*, 1733–1734.
(6) Osawa, M.; Hoshino, M.; Hashizume, D. *Dalton Trans.* **2008**, 2248–2252.
(7) Ma, Y.; Zhou, X.; Shen, J. *Appl. Phys. Lett.* **1999**, *74*, 1361–1363.
(8) Wang, H. M. J.; Chen, C. Y. L.; Lin, I. J. B. *Organometallics* **1999**, *18*, 1216–1223.
(9) Forward, J. M.; Bohmann, D. B.; Fackler, J. J. P.; Staples, R. J. *Inorg. Chem.* **1995**, *34*, 6330–6336.
(10) Schmidbaur, H.; Schier, A. *Chem. Soc. Rev.* **2008**, *37*, 1931–1951.
(11) Pyykkö, P. *Angew. Chem., Int. Ed.* **2004**, *43*, 4412–4456.
(12) Evans, R. C.; Douglas, P.; Winscom, C. J. *Coord. Chem. Rev.* **2006**, *250*, 2093–2126.
(13) Yam, V.-W.; Chan, C.-L.; Li, C.-K.; Wong, K.-C. *Coord. Chem. Rev.* **2001**, *216*−*217*, 173–194.


Published on Web 07/22/2010

Chart 1

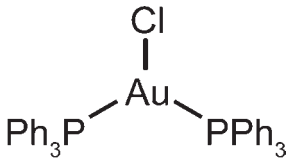


yellow by a grinding-induced crystal−amorphous phase transition.[14] This alteration in emission color is related to the change in the intermolecular distance between two Au centers; molecules are discrete in the crystalline state, whereas they form dimer structures by aurophilic interactions in the amorphous state. Another color alteration study was reported by Kishimura et al. They focused on $[Au_3\{(C18)pz\}_3]$ ($\{(C18)pz\}^-$ = 4-(3,5-dioctadecyloxybenzyl)-3,5-dimethylpyrazolate anion) and showed that the color alteration of this complex was induced by a change in the Au···Au geometry by a solid-gel phase transition or the addition of $Ag^+$.[15]

For the three-coordinated Au(I) complexes, $[AuL_3]$, the emission was predicted on the basis of the large structural change induced by the $p\sigma \leftarrow d\sigma^*$ electron transition.[4,5] McCleskey and Gray studied the photoexcited structure spectroscopically and reported that shrinkage of the $[AuL_3]$ unit was induced by photoexcitation.[5] On the other hand, Omary et al. reported the calculated lowest triplet state photoexcited structure of various $[AuL_3]$ complexes.[16,17] All of the structures suggested that distortion from a triangle to a T-shaped structure was induced by photoexcitation. Because of this discrepancy, the principle of emission from $[AuL_3]$ has not been fully understood yet.

Recently, we reported the photoexcited structure of the three-coordinated Au(I) complex, $[AuCl(PPh_3)_2]$ (Chart 1), using the novel photocrystallographic method, the photostable X-ray diffraction method.[18,19] In this method, diffraction data are collected with and without photoirradiation. Structural change by photoirradiation is examined by comparing results of the crystal structure analysis for each of the intensity data sets. The observed structural change of $[AuCl(PPh_3)_2]$ on photoexcitation corresponded to Gray's model; the shortening of every metal−ligand bond was induced by photoexcitation. This work revealed that the shrinkage of the molecule by photoexcitation is the origin of the green phosphorescence of the $[AuCl(PPh_3)_2]$ crystal. Moreover, the effect of the crystal structure change on the photoexcited structure and the emission color was examined by temperature-dependent photocrystallographic analysis and spectroscopic measurements.[18] These results indicated that the shrinkage of the crystal structure by cooling induced structural and energetic changes in $[AuCl(PPh_3)_2]$, and, as a result, a red-shift of the emission was observed (~20 nm with cooling from 295 to 75 K). This work led to the novel emission-control idea: the emission color of $[AuCl(PPh_3)_2]$ could be controlled by changing the environment around the molecule in the crystal, for example, by growing a polymorphic crystal.

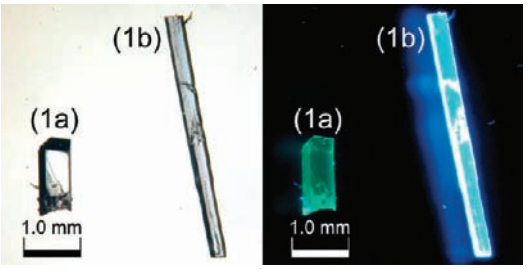


**Figure 1.** Single crystals and emission of **1a** and **1b**: the left-hand panel is under room light and the right-hand panel is under UV-irradiation (313, 334, and 365 nm from an ultrahigh pressure mercury lamp with an optical filter).

After several trials, we succeeded in obtaining the novel polymorphic crystal of $[AuCl(PPh_3)_2]$ by controlling the growth rate of the crystal. The pictures of the known and novel polymorphic crystals (**1a** and **1b**) showing their emission under UV-irradiation are shown in Figure 1. Although the polymorphic crystals contain the same molecule, they showed quite different emission colors (green and blue). This color difference suggests that the structural change by photoexcitation of $[AuCl(PPh_3)_2]$ in **1b** is not the metal−ligand bond-shortening as in **1a**, and that this is due to their differences in molecular environment in the crystal. So, the aim of this study was the direct observation of the photoexcited structure of $[AuCl(PPh_3)_2]$ in **1b** and the elucidation of the principle behind the emission color change, using the photostable X-ray diffraction method, spectroscopy, and theoretical calculations. The photostable X-ray diffraction experiments were performed not only in a laboratory system but also at a synchrotron facility (SPring-8 BL02B1) to collect high-precision data and to analyze in detail the electron density change by photoexcitation.

## Experimental Section

**Preparation of the Single Crystal of 1b.** The two-coordinated complex $[AuCl(PPh_3)]$ was synthesized using the reported method.[20] $[AuCl(PPh_3)]$ and an equimolar amount of triphenylphosphine were dissolved in hot acetonitrile and saturated by heating in a hot-water bath. After filtering a small amount of residual powder, the solution was left at room temperature. The suitable needle-like single crystals of **1b** were obtained in an hour or two.

**Measurements of the Absorption and Emission Spectra and Selection of Excitation Light. 1b** (7 mg) was mixed with $BaSO_4$ (350 mg) and ground well. The mixture powder was packed into a sample holder, and a diffuse reflectance spectrum was collected using a JASCO V-560 spectrometer equipped with an integrating sphere accessory. The spectrum was converted to a UV−vis absorption spectrum by using the Kubelka−Munk equation. The converted spectrum is shown in Figure 2.

For measurements of emission spectra, a few crystals of sample were attached to a coldfinger of a cryostat and cooled by a closed cycle helium compressor system. Measurements were performed every 20 K between 280 and 60 K and every 10 K between 60 and 10 K.

For the excitation light to penetrate the single-crystalline sample, the wavelength of the light has to correspond roughly to the edge of its absorption band.[21] So, an ultrahigh pressure mercury lamp with an optical glass filter (TOSHIBA UV-D33S)

(14) Ito, H.; Saito, T.; Oshima, N.; Kitamura, N.; Ishizaka, S.; Hinatsu, Y.; Wakeshima, M.; Kato, M.; Tsuge, K.; Sawamura, M. *J. Am. Chem. Soc.* **2008**, *130*, 10044–10045.
(15) Kishimura, A.; Yamashita, T.; Aida, T. *J. Am. Chem. Soc.* **2005**, *127*, 179–183.
(16) Sinha, P.; Wilson, A. K.; Omary, M. A. *J. Am. Chem. Soc.* **2005**, *127*, 12488–12489.
(17) Barakat, K. A.; Cundari, T. R.; Omary, M. A. *J. Am. Chem. Soc.* **2003**, *125*, 14228–14229.
(18) Hoshino, M.; Uekusa, H.; Sonoda, S.; Otsuka, T.; Kaizu, Y. *Dalton Trans.* **2009**, 3085–3091.
(19) Hoshino, M.; Uekusa, H.; Ohashi, Y. *Bull. Chem. Soc. Jpn.* **2006**, *79*, 1362–1366.
(20) Gregory, B. J.; Ingold, C. K. *J. Chem. Soc. B* **1969**, 276–289.
(21) Enckelmann, V.; Wegner, G. J. *J. Am. Chem. Soc.* **1993**, *115*, 10390–10391.

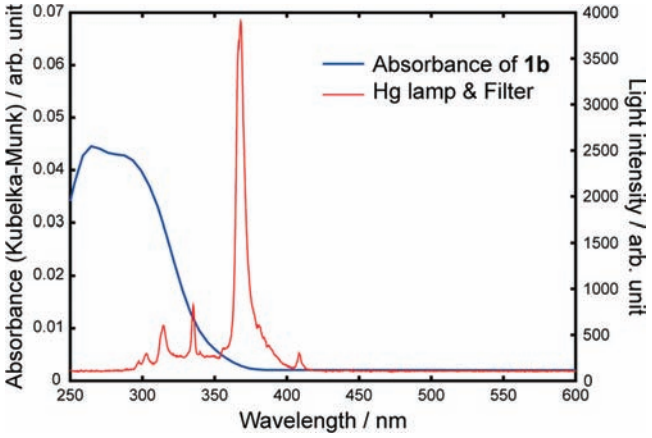


**Figure 2.** Absorbance of **1b** (blue line) and the wavelength distribution of a Hg lamp with an optical filter (red line).

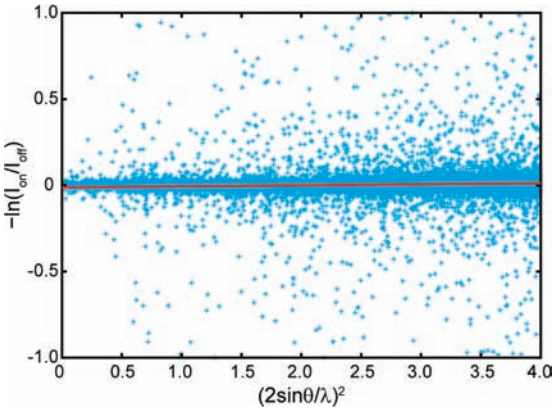


**Figure 3.** Wilson-type plot of $(2 \sin \theta/\lambda)^2$ versus $-\ln (I_{on}/I_{off})$. The red line is the linear fitted function.

was selected as the excitation light source for the X-ray diffraction experiment in a laboratory system (the wavelength distribution is shown in Figure 2) and an He−Cd laser ($\lambda$ = 325 nm, 30 mW) was selected for the synchrotron X-ray diffraction experiment at SPring-8 BL02B1.

**Single Crystal X-ray Diffraction Experiment.** A single crystal of dimensions 0.38 × 0.15 × 0.10 mm was used for the X-ray diffraction experiment in a laboratory system. Diffraction intensity measurements under photoirradiation (light-on) and non-irradiation (light-off) conditions were performed at three low temperatures (182, 144, and 102 K). All data were collected on a Rigaku R-AXIS Rapid equipped with a rotating anode X-ray source (Mo Kα radiation, $\lambda$ = 0.71073 Å) and a Rigaku nitrogen-gas stream temperature control system. Sets of data frames (0° to 160°, $\omega$ scan) were collected at four $\varphi$ orientations (0°, 90°, 180°, and 270°), and the $\chi$ arm was fixed at 45°. The integration and scaling of collected data were processed by the programs DENZO and SCALEPACK, respectively.[22] Semiempirical absorption correction was performed on PLATON-MULABS.[23] All structures were solved by direct methods (SHELXS-97) and refined by the full-matrix least-squares method (SHELXL-97).[24] All the non-hydrogen atoms were refined with anisotropic temperature factors. All the hydrogen atoms were found in the difference Fourier map and refined isotropically using $U_{iso} = 1.2U_{eq}$ of the connected carbon atom.

For the synchrotron X-ray diffraction experiment at SPring-8 BL02B1, a single crystal was shaped to the dimensions 0.17 × 0.12 × 0.05 mm, and the shortest dimension was oriented to the direction of the laser irradiation. X-ray diffraction data of the light-off and light-on stages (−90° to 100°, $\varphi$ scan) were collected using the high-accuracy photostable X-ray diffraction method, the multiple-exposure imaging plate (IP) method, on a low-temperature vacuumed X-ray camera.[25] A monochromatic X-ray ($\lambda$ = 0.55636 Å, Si(311) double crystal monochromator) was used, and the crystal was cooled at 29 K by a cryostat system with a helium compressor. To minimize the temperature difference caused by laser irradiation between the light-off and the light-on stages, both stages were arranged by chopped X-ray and excitation light generated by rotating shutters (rotating speed = 50 Hz); X-ray and excitation light were synchronized in the light-on stage, and photoirradiation was performed during the closed X-ray shutter period in the light-off stage. Using this exposure system, the sample was warmed up because of laser irradiation was the same in both stages. The methods of data processing and structural analysis were the same as for the laboratory system. All the non-hydrogen atoms were refined with anisotropic temperature factors. All the hydrogen positions were calculated and refined using the riding-model by the HFIX command on SHELXL-97. Crystallographic information files for all of crystal structures were submitted to CCDC (reference numbers 745565−745572).

**Analysis of Electron Density Change by Photoexcitation.** Electron density change by photoexcitation was analyzed based on the photodifference Fourier synthesis map.[26] The map was drawn by using the coefficient of the difference of the observed structure factors ($F_o$) between the light-off and light-on stage, which was obtained by the structural analysis of the data collected at SPring-8 BL02B1. Change in the overall isotropic temperature factor ($\Delta B$) by laser irradiation was estimated by the Wilson-type plot from the diffraction intensities of the light-off and light-on stages and was used as the correction term to $F_o$ of the light-on stage.[27] The result of the Wilson-type plot is shown in Figure 3. The slope of the linear-fit to the Wilson-type plot led to the derivation of $\Delta B/2$ = 0.006132 ± 0.002496. This value was within the experimental error ($3\sigma$). Thus, the temperature heating effect by laser-irradiation was probably negligible. But to draw the most precise and accurate photodifference Fourier map possible, it was used to correct the $B$ factor in $F_o$ in the light-on stage.

Integration of electron densities around Au and Cl in the photodifference Fourier map and conversion of these to atomic charges were carried out by the program CHARGE in the Xtal 3.7 program suite.[28] The integration range was defined as within the effective ionic radii (Au: 1.37 Å, Cl: 1.81 Å).[29]

**Computational Methods.** All density functional theory (DFT) calculations were carried out using the program GAUSSIAN 03.[30]

(22) Otwinowski, Z.; Minor, W. *Methods Enzymol*. **1997**, *276*, 307−326.
(23) Spek, A. L. *J. Appl. Crystallogr*. **2003**, *36*, 7–13.
(24) Sheldrick, G. M. *Acta Crystallogr*. **2008**, *A64*, 112–122.
(25) Ozawa, Y.; Terashima, M.; Mitsumi, M.; Toriumi, K.; Yasuda, N.; Uekusa, H.; Ohashi, Y. *Chem. Lett*. **2003**, *32*, 62–63.
(26) Carducci, M. D.; Pressprich, M. R.; Coppens, P. *J. Am. Chem. Soc*. **1997**, *119*, 2669–2678.
(27) Ozawa, Y.; Pressprich, M. R.; Coppens, P. *J. Appl. Crystallogr*. **1998**, *31*, 128–135.
(28) Spadaccini, N. *CHARGE, Xtal3.7 System*, 2000.
(29) Shannon, R. D. *Acta Crystallogr*. **1976**, *A32*, 751–767.
(30) Frisch, M. J.; Trucks, G. W.; Schlegel, H. B.; Scuseria, G. E.; Robb, M. A.; Cheeseman, J. R.; Montgomery, Jr., J. A.; Vreven, T.; Kudin, K. N.; Burant, J. C.; Millam, J. M.; Iyengar, S. S.; Tomasi, J.; Barone, V.; Mennucci, B.; Cossi, M.; Scalmani, G.; Rega, N.; Petersson, G. A.; Nakatsuji, H.; Hada, M.; Ehara, M.; Toyota, K.; Fukuda, R.; Hasegawa, J.; Ishida, M.; Nakajima, T.; Honda, Y.; Kitao, O.; Nakai, H.; Klene, M.; Li, X.; Knox, J. E.; Hratchian, H. P.; Cross, J. B.; Bakken, V.; Adamo, C.; Jaramillo, J.; Gomperts, R.; Stratmann, R. E.; Yazyev, O.; Austin, A. J.; Cammi, R.; Pomelli, C.; Ochterski, J. W.; Ayala, P. Y.; Morokuma, K.; Voth, G. A.; Salvador, P.; Dannenberg, J. J.; Zakrzewski, V. G.; Dapprich, S.; Daniels, A. D.; Strain, M. C.; Farkas, O.; Malick, D. K.; Rabuck, A. D.; Raghavachari, K.; Foresman, J. B.; Ortiz, J. V.; Cui, Q.; Baboul, A. G.; Clifford, S.; Cioslowski, J.; Stefanov, B. B.; Liu, G.; Liashenko, A.; Piskorz, P.; Komaromi, I.; Martin, R. L.; Fox, D. J.; Keith, T.; Al-Laham, M. A.; Peng, C. Y.; Nanayakkara, A.; Challacombe, M.; Gill, P. M. W.; Johnson, B.; Chen, W.; Wong, M. W.; Gonzalez, C.; and Pople, J. A. *Gaussian 03*, Revision D.02; Gaussian,Inc.: Wallingford, CT, 2004.

**Table 1.** Crystallographic Data from the Laboratory System Measurement

| | 182Koff (light-off) | 182Kon (light-on) | 144Koff (light-off) | 144Kon (light-on) | 104Koff (light-off) | 104Kon (light-on) |
|---|---|---|---|---|---|---|
| temperature (K) | 182(2) | 182(2) | 144(2) | 144(2) | 104(2) | 104(2) |
| $a$ (Å) | 24.7893(3) | 24.7774(3) | 24.7218(3) | 24.7152(3) | 24.6707(3) | 24.6711(3) |
| $b$ (Å) | 9.0436(1) | 9.0437(1) | 9.0413(1) | 9.0411(1) | 9.0393(1) | 9.0394(1) |
| $c$ (Å) | 15.0336(2) | 15.0307(3) | 14.9853(2) | 14.9843(2) | 14.9426(2) | 14.9409(2) |
| $\beta$ (deg) | 117.2979(9) | 117.2489(9) | 117.2049(8) | 117.1805(9) | 117.1342(8) | 117.1357(8) |
| $V$ (Å$^3$) | 2994.96(6) | 2994.30(8) | 2978.94(6) | 2978.54(6) | 2965.54(6) | 2965.24(6) |
| $\mu$ (mm$^{-1}$) | 5.13 | 5.13 | 5.16 | 5.16 | 5.18 | 5.18 |
| $T_{min}$ | 0.197 | 0.195 | 0.194 | 0.195 | 0.193 | 0.192 |
| $T_{max}$ | 0.271 | 0.271 | 0.270 | 0.269 | 0.267 | 0.268 |
| no. of measured reflections | 51928 | 51377 | 51339 | 51418 | 51279 | 51311 |
| no. of independent reflections | 5235 | 5242 | 5202 | 5201 | 5187 | 5187 |
| no. of observed reflections | 5203 | 5202 | 5180 | 5178 | 5172 | 5169 |
| $R_{int}$ | 0.032 | 0.033 | 0.032 | 0.033 | 0.034 | 0.034 |
| $\theta_{max}$ (deg) | 32.1 | 32.1 | 32.1 | 32.1 | 32.1 | 32.1 |
| $R[F^2 > 2\sigma(F^2)]$ | 0.017 | 0.017 | 0.017 | 0.017 | 0.017 | 0.017 |
| $wR(F^2)$ | 0.044 | 0.044 | 0.045 | 0.044 | 0.042 | 0.043 |
| $S$ | 1.14 | 1.15 | 1.17 | 1.15 | 1.14 | 1.16 |
| no. of parameters | 227 | 227 | 227 | 227 | 227 | 227 |

**Table 2.** Crystallographic Data of the SPring-8 BL02B1 Measurement

| | 29Koff (light-off) | 29Kon (light-on) |
|---|---|---|
| temperature (K) | 29(2) | 29(2) |
| $a$ (Å) | 24.6370(2) | 24.6380(2) |
| $b$ (Å) | 9.0440(1) | 9.0440(1) |
| $c$ (Å) | 14.9050(2) | 14.9050(2) |
| $\beta$ (deg) | 117.0610(5) | 117.0610(5) |
| $V$ (Å$^3$) | 2957.50(6) | 2957.62(6) |
| $\mu$ (mm$^{-1}$) | 2.83 | 2.83 |
| $T_{min}$ | 0.617 | 0.617 |
| $T_{max}$ | 0.681 | 0.679 |
| no. of measured reflections | 43284 | 43227 |
| no. of independent reflections | 11935 | 11900 |
| no. of observed reflections | 11359 | 11329 |
| $R_{int}$ | 0.032 | 0.032 |
| $\theta_{max}$ (deg) | 33.8 | 33.8 |
| $R[F^2 > 2\sigma(F^2)]$ | 0.020 | 0.020 |
| $wR(F^2)$ | 0.083 | 0.081 |
| $S$ | 1.24 | 1.20 |
| no. of parameters | 183 | 183 |

Optimized structures of the $S_0$ and $T_1$ states were obtained by using the B3LYP functional with LanL2DZ ECP and basis set for Au and 6-31G* basis set for other atoms. Optimization calculations were performed under the geometrical constraint of the 2-fold symmetry. Mulliken atomic charges at the ground and photoexcited states were obtained by single-point energy calculation with the same functional and basis sets. In this calculation, for the photoexcited state in **1b** it was assumed that an electron transited to the second lowest unoccupied molecular orbital (LUMO+1) without any structural change from the optimized structure of the $S_0$ state. The difference between the squared molecular orbitals (MOs), which was used in the charge calculation above, was applied to simulate the photodifference Fourier map. Time-dependent (TD)-DFT calculations for the optimized $S_0$ and $T_1$ states geometry with the same functional, ECP, and basis sets were also carried out.

## Results and Discussion

**Crystal Structure.** Crystallographic data from the laboratory system and the synchrotron experiment are shown in Tables 1 and 2, respectively. **1b** belongs to the monoclinic crystal system (space group: $C2/c$), and four molecules are included in a unit cell. The Au−Cl bond is on the crystallographic 2-fold axis, and so half of the molecule is independent in an asymmetric unit ($Z' = 1/2$). The molecular and crystal structures of **1b** are shown in Figures 4 and 5, respectively. The crystal structures of **1b** and **1a** are completely different;[18] **1b** is constructed based on a one-dimensional (1D) chain motif, whereas **1a** has an aggregate structure of a weakly linked dimer motif with C−H···Cl interactions (Figure 6).

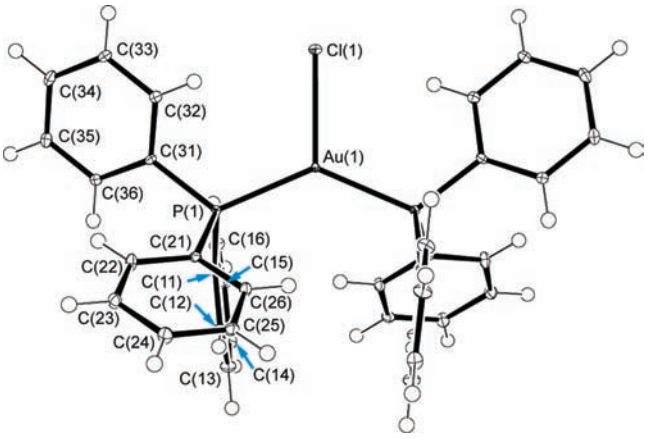


**Figure 4.** ORTEP diagram of [AuCl(PPh$_3$)$_2$] in **1b** at 29 K (light-off), showing atoms with 50% thermal ellipsoids.

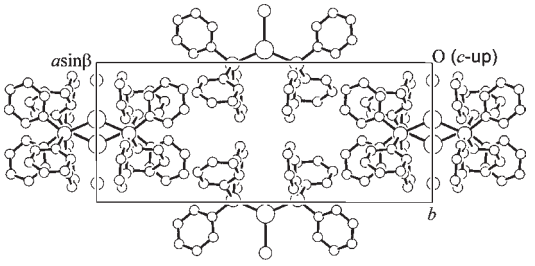


**Figure 5.** Crystal structure of **1b** viewed along the $c$ axis.

**Direct Observation of the Photoexcited Structure of [AuCl(PPh$_3$)$_2$].** In our previous work on **1a** and the solvated crystal, [AuCl(PPh$_3$)$_2$]·CHCl$_3$, shortening of every metal−ligand bond by photoexcitation caused shrinkage of the crystal lattice.[18,19] So the change of the unit-cell volume by photoirradiation was examined first (Table 3). In spite of significant shrinkage ($V_{on} - V_{off} \leq -10$ Å$^3$) in **1a** and the solvated crystal, the volume change of **1b** was within ±1 Å$^3$ at all temperatures. Moreover, changes of bond lengths, bond angles, and torsion angles at all temperatures remained

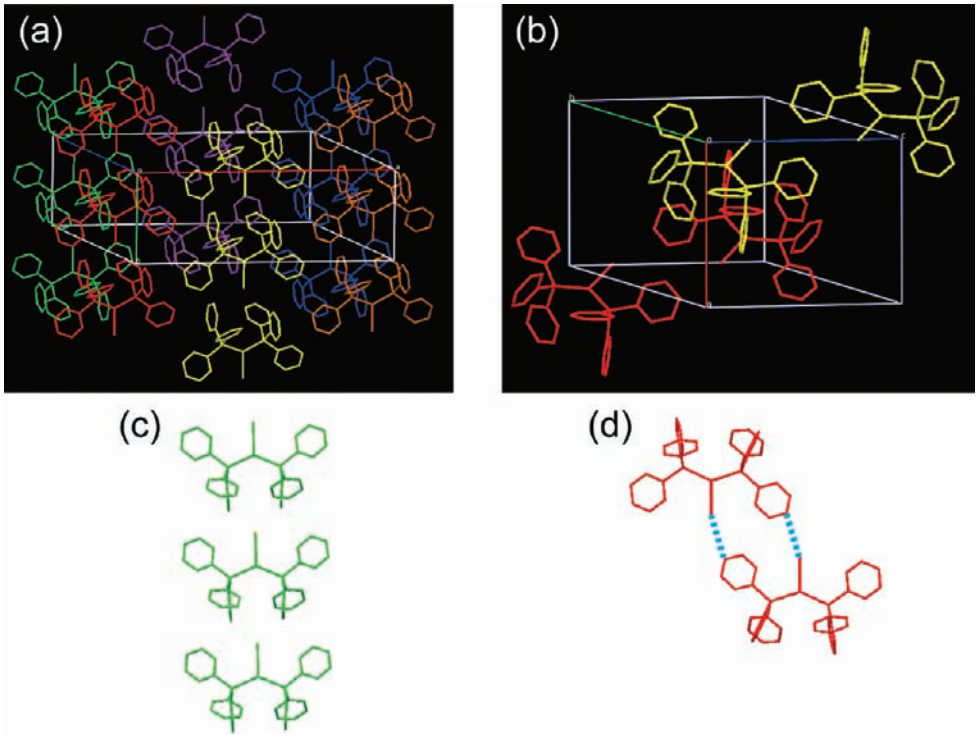


**Figure 6.** (a) Crystal structure of **1b**. (b) Crystal structure of **1a**.[18] (c) 1D chain motif in **1b**. (d) Weakly linked dimer motif in **1a**.[18] The independent motif is distinguished by color-coding, and C−H···Cl interactions are shown as blue dotted lines in (d).

**Table 3.** Temperature-Dependent Change of the Cell Volume (Å$^3$)

| | light-off stage | light-on stage | $\Delta_{on-off}$[a] |
|---|---|---|---|
| 182 K | 2994.96 (6) | 2994.30 (8) | −0.66(8) |
| 144 K | 2978.94 (6) | 2978.54 (6) | −0.40(6) |
| 104 K | 2965.54 (6) | 2965.24 (6) | −0.30(5) |
| 29 K | 2957.50 (6) | 2957.62 (6) | +0.12(6) |

[a] Difference between the light-on and light-off stage (estimated standard deviations are larger in the calculation).

within the experimental errors (lower than three times the standard uncertainty, see Supporting Information). This means that the difference in the geometry of $[AuCl(PPh_3)_2]$ in **1b** between the ground and the photoexcited state was too small to be examined by typical X-ray structural analysis. Therefore, a more detailed analysis was necessary to observe the slight change caused by photoexcitation.

So, the electron density change caused by photoexcitation was examined based on the photodifference Fourier map (Figure 7). Decreases in electron densities around Au and Cl were observed, and no other noticeable electron density peak was observed around the molecule. To examine these electron density decreases in detail, a comparison with the results of the spectroscopic measurements and theoretical calculations was made. The ordering of the MOs in the $S_0$ and $T_1$ states obtained by DFT calculations are summarized in Figure 8. Because the two highest occupied MOs (HOMOs) were close energetically (the difference in energy between these being 0.0014 eV), these MOs were referred to as HOMO(1) and HOMO(2), respectively. The optimized $S_0$ state geometry almost corresponded with the molecular structure by crystallographic analysis. Selected bond lengths and bond angles are tabulated in Table 4. Distribution of the MOs in the $S_0$ and $T_1$ states clearly indicated that the lowest triplet state of $[AuCl(PPh_3)_2]$ is the photoexcited "shrunk" structure observed in our previous studies in **1a** and the solvated crystal;[18,19] the shortening of every metal−ligand bond was induced by the electron transition accompanied by the weakening of the HOMO-(1)'s antibonding character around the Au−Cl bond and the strengthening of the LUMO's bonding character around the Au−P bonds. (see Supporting Information)

On the other hand, because **1b** showed shorter-wavelength phosphorescence than **1a**, an electron should transit to an energetically higher orbital than the LUMO in **1b**. Vertical transition (triplet ← singlet) energies obtained by TD-DFT calculations suggested that the excited state with the LUMO+1 ← HOMO(1) transition accounted for the blue emission from **1b** (triplet ← singlet transition energy was 429 nm in wavelength). But the excited state with the LUMO+2 ← HOMO(1) transition may also generate the blue emission (triplet ← singlet transition energy was 404 nm in wavelength). To decide which excited state contributes the blue emission, the temperature dependence of the emission spectrum of **1b** was examined (Figure 9; the spectral peaks are tabulated in the Supporting Information). The emission peak was found at $\lambda_{max}$ = 457 nm at 280 K, but this emission band gradually became weaker, while the other emission band ($\lambda_{max}$ = 473 nm) gradually became stronger with cooling. This dependence means that deactivation from the excited state with the LUMO+2 ← HOMO(1) transition was allowed and dominated the blue emission ($\lambda_{max}$ = 457 nm) at the high-temperature region (higher than ∼140 K), but below 140 K almost all transiting electrons reached the more stable MO, LUMO+1, and deactivated from this excited state with the relatively long-wavelength emission ($\lambda_{max}$ = 473 nm). This type of change of the emission-dominating MO is not common. But a similarly temperature-dependent change of an emission path has

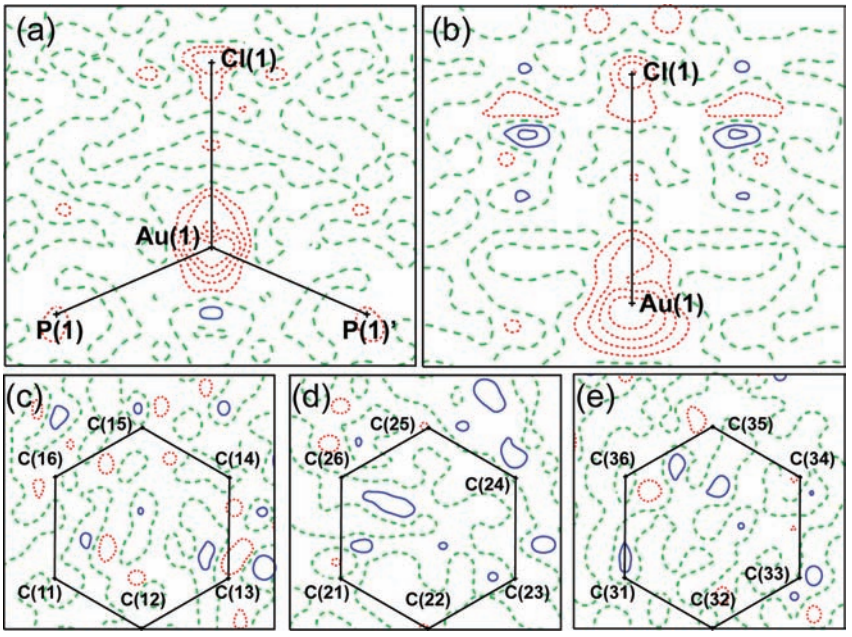


**Figure 7.** Photodifference Fourier maps, representing electron density change by photoexcitation at 29 K: (a) map containing Au, P, and Cl; (b) map perpendicular to the plane containing Au, P, and Cl; (c, d, e) maps of phenyl rings (blue lines: positive; red dotted lines: negative; contour level: 0.5 e $Å^{-3}$).

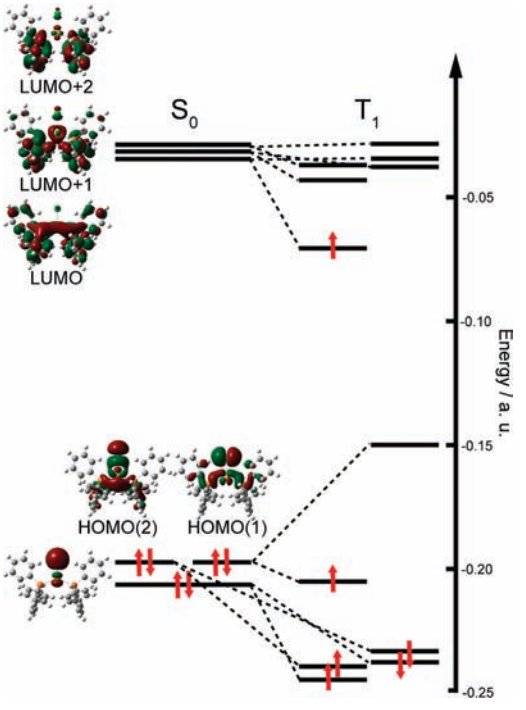


**Figure 8.** Ordering of MOs in the $S_0$ and $T_1$ states in $[AuCl(PPh_3)_2]$ (the isosurface of each MO is 0.02 au).

been observed in $Cu_4L_4X_4$ clusters and $\{[3,5\text{-}(i\text{-}Pr)_2Pz]\text{-}Cu\}_3$.[31−33] These examples support the suggested change of emission path above. So, the photodifference Fourier map created by using the data collected at 29 K reflected the photoexcited structure with electron transition from

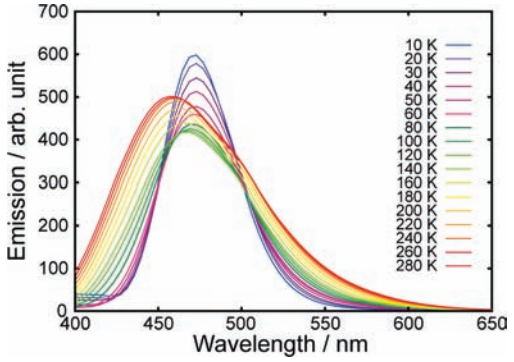


**Figure 9.** Temperature dependence of the emission spectrum of **1b**. The temperatures for the colored line are defined in the figure.

**Table 4.** Selected Bond Lengths and Bond Angle at the Ground State Obtained by Crystallographic Analysis and Theoretical Calculations

| | Au−P/Å | Au−Cl/Å | P−Au−P/deg |
|---|---|---|---|
| 182Koff | 2.3215 (3) | 2.5257 (6) | 133.015 (17) |
| 144Koff | 2.3202 (3) | 2.5268 (6) | 133.100 (17) |
| 104Koff | 2.3196 (3) | 2.5282 (5) | 133.207 (17) |
| 29Koff | 2.3222 (4) | 2.5349 (6) | 133.36 (2) |
| optimized $S_0$ geometry | 2.427 | 2.594 | 137.36 |

HOMO(1) to LUMO+1. Additionally, oscillator strengths ($f$) established by TD-DFT calculation for the optimized $S_0$ state structure provided that electron transitions from HOMO(1) to LUMO ($\lambda_{calc}$ = 330 nm, $f$ = 0.0257), LUMO+1 ($\lambda_{calc}$ = 319 nm, $f$ = 0.0129), and LUMO+2 ($\lambda_{calc}$ = 310 nm, $f$ = 0.0346) are probable.

HOMO(1) was, as already mentioned, the antibonding orbital around the Au−Cl bond. And LUMO+1 was mainly contributed by the $\pi^*$ orbital in two $PPh_3$ ligands. These MOs suggested that the blue emission from **1b** relates to the photoexcited charge-transferred state from the Au−Cl moiety to the $PPh_3$ ligands. Consideration of the photodifference Fourier map based on the suggested charge-transferred state leads to the conclusion that the

(31) Ford, P. C.; Cariati, E.; Bourassa, J. *Chem. Rev.* **1999**, *99*, 3625–3648.
(32) Vitale, M.; Ryu, C. K.; Palke, W. E.; Ford, P. C. *Inorg. Chem.* **1994**, *33*, 561–566.
(33) Dias, H. V. R.; Diyabalanage, H. V. K.; Eldabaja, M. G.; Elbjeirami, O.; Rawashdeh-Omary, M. A.; Omary, M. A. *J. Am. Chem. Soc.* **2005**, *127*, 7489–7501.

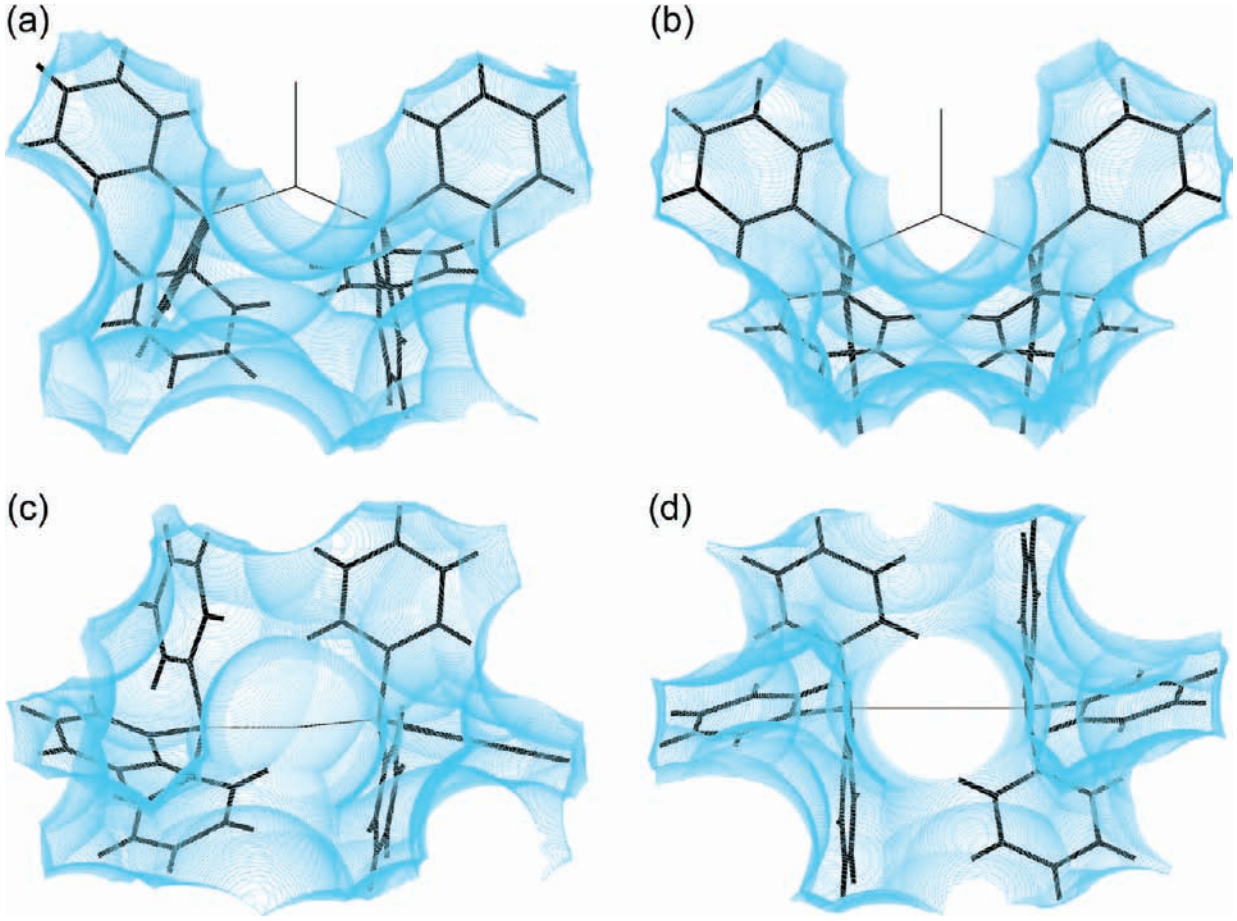


**Figure 10.** Reaction cavities around $PPh_3$ ligands: (a) in **1a**, view toward the plane containing Au, P, and Cl; (b) in **1b**, view toward the plane containing Au, P, and Cl; (c) in **1a**, view along the direction from Au to Cl; (d) in **1b**, view along the direction from Au to Cl.

decreases in electron density around Au and Cl in the map reflect the charge transfer from the Au−Cl moiety to the $\pi^*$ orbitals in the two $PPh_3$ ligands and, because of the significantly weaker contribution of a delocalized electron to diffraction, transferred charge becomes unnoticeable because of the delocalization in the $\pi$ conjugation system of a phenyl ring (Figure 7).

The above discussion clearly demonstrates the charge-transferred nature of the photoexcited structure in **1b**. And the difference in the generated photoexcited structures of **1a** and **1b** explains why the emission colors of these crystals were completely different.

**Relationship between Emission Color and Crystal Structure of [AuCl($PPh_3$)$_2$].** Because both **1a** and **1b** contain the same molecule, the difference in their crystal structures would account for the difference in structural change brought about by photoexcitation (bond shortening or charge transfer). To examine the effect of the crystal structure on structural change by photoexcitation, an environment around a molecule in a crystal was visualized using a reaction cavity drawing.[34] The reaction cavity is the available space for photoinduced movement of atoms or functional groups in a crystal and is often used to elucidate details of crystalline-state photoreaction.[35−38] In the present study, the reaction cavities around the $PPh_3$ ligands in **1a** and **1b** (the light-off stage at 118 and 104 K, respectively) were calculated to examine the accessible space for the photoinduced movement of each $PPh_3$ (Figure 10). The reaction cavity drawing of **1b** showed an inaccessible region along the Au−Cl bond (a central blank area in Figure 10d). This means that the $PPh_3$ ligands cannot move toward the Au−Cl moiety in **1b**. This region is formed because of the 1D chain motif in **1b**, in which the Cl moiety is arranged in the P−Au−P angle of the neighboring molecule (Figure 6c). As mentioned above, the lowest triplet state structure of an ideal isolated [AuCl($PPh_3$)$_2$] in vacuum, obtained by DFT calculations, was generated by an electron transition to the LUMO with shortening of the Au−P (and Au−Cl) bonds. The reaction cavity in **1a**, which includes the area around the Au−Cl bond (Figure 10c), allowed the shortening of the Au−P bonds to reach the lowest triplet state sterically in this crystal. Because of this reaction cavity, the photoexcited "shrunk" structure can be generated, and a green emission was observed from **1a**. In contrast, the reaction cavity in **1b**, which shows the inaccessible region along the Au−Cl bond, expresses the inhibition of the energetic stabilization by shortening of the Au−P bonds sterically in this crystal. Therefore, the

(34) Ohashi, Y.; Yanagi, K.; Kurihara, T.; Sasada, Y.; Ohgo, Y. *J. Am. Chem. Soc.* **1981**, *103*, 5805–5812.
(35) Hosoya, T.; Uekusa, H.; Ohashi, Y.; Ohhara, T.; Tanaka, I.; Niimura, N. *Acta Crystallogr.* **2006**, *B62*, 153–160.
(36) Naumov, P.; Ohashi, Y. *Acta Crystallogr.* **2004**, *B60*, 343–349.
(37) Takayama, T.; Kawano, M.; Uekusa, H.; Ohashi, Y.; Sugawara, T. *Helv. Chim. Acta* **2003**, *86*, 1352–1358.
(38) Ohashi, Y. *Acc. Chem. Res.* **1988**, *21*, 268–274.

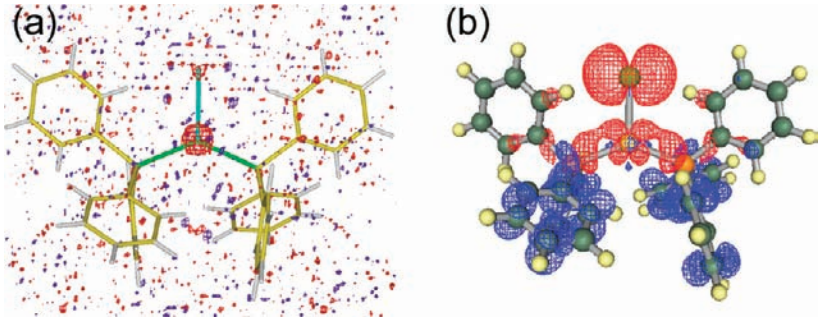


**Figure 11.** Three-dimensional photodifference Fourier maps: (a) experimental map at 29 K with ±0.7 e $Å^{-3}$ isosurface level; (b) theoretical map corresponding to 100% conversion with ±0.001 au isosurface level (blue: positive, red: negative).

**Table 5.** Changes in the Atomic Charge of Au and Cl by Charge Transfer

| | by integration | by simulation |
|---|---|---|
| Au | +1.290 | +0.005 |
| Cl | +0.062 | +0.655 |

LUMO, which relates to shortening of the Au−P bonds, becomes unstable, and the LUMO+1, which relates to charge transfer, behaves as the LUMO in **1b**. For this reason, there was not a green but a blue emission observed from **1b**. In summary, it is seen that the photoexcited structure and emission color of $[AuCl(PPh_3)_2]$ depended on the packing motif of the crystal structure, or the environment surrounding the molecule in the crystal.

**Population of Excited Molecules.** In other crystallographic studies of photoexcited molecules, the population of the excited molecule in the crystal was determined by using the special least-squares refinement technique.[25,39−42] In this technique, the disordered model including the ground and excited molecules was refined using the specially defined parameter, the response ratio.[27] But in the present case, applying this technique was impossible because the structural difference between ground and photoexcited molecule was too small to construct and refine the disordered model. So the population was estimated by examining the change in atomic charge.

Changes of the atomic charge of Au and Cl were calculated by integration of electron densities based on the ionic radii in the photodifference Fourier map and comparing these with values simulated by DFT calculations (Table 5). Because the integrated and simulated changes of the atomic charges of Au and Cl were positive, charge transfer from the Au−Cl moiety by photoexcitation was qualitatively confirmed. But from a quantitative aspect, the integrated value of Au (+1.290) was significantly larger than the simulated value (+0.005) and corresponded to more than one electron transition. To examine this anomalous integrated value, simulated photodifference Fourier maps corresponding to the electron transition from HOMO(1) to LUMO+1 were

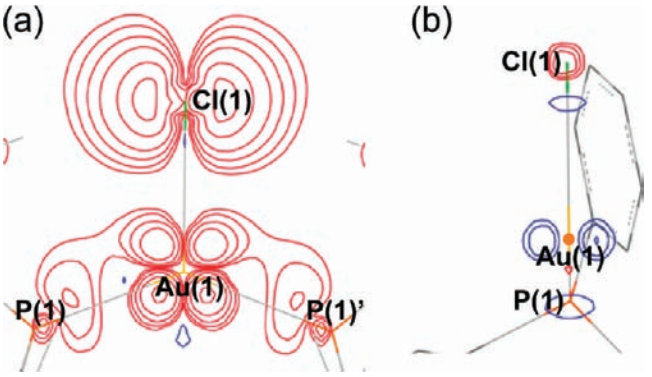


**Figure 12.** Photodifference Fourier maps corresponding to 100% conversion from DFT calculation: (a) map containing Au, P, and Cl; (b) map containing Au and Cl, perpendicular to the plane (a). (Blue lines: positive, red lines: negative, contours: ±0.001, ±0.002, ±0.004, −0.008, −0.02, and −0.04 au).

calculated and compared with experimental maps. The three-dimensional experimental and theoretical difference map (Figure 11) showed a decrease in electron densities around Au and Cl. In the experimental photodifference map, the electron density decrease on Au was observed more clearly than that on Cl because the larger scattering factor and smaller thermal vibration of Au would contribute to produce clearer electron density around Au. Positive regions around the triphenylphosphines in Figure 11b clearly showed that the transferred electron was delocalized in the $\pi$ conjugation system and could not be observed in the experimental map (Figure 11a). So this theoretical map can be regarded as reliable for comparison with the experimental one. Difference maps containing Au, P, and Cl (Figures 7a and 12a) also qualitatively agreed. In contrast, the electron densities of Au in the perpendicular direction of the plane containing Au, P, and Cl were completely different; positive peaks around Au in the simulated map did not appear in the experimental map (Figures 7b and 12b). The reason for this difference would be the slight structural change of Au or the effect of the series termination error in the Fourier summation. So, the change in atomic charge of Au would not be appropriate for estimation of the population.

On the other hand, electron densities around Cl in the experimental and simulated maps were approximately the same. So the atomic charge of Cl would be better for estimation of the population than that of Au. From comparison with the simulated value (+0.655), which corresponds to 100% photoexcitation in the crystal, the integrated value (+0.062) indicates that about 9% of the photoexcited

(39) Vorontsov, I. I.; Kovalevsky, A. Y.; Chen, Y. -S.; Graber, T.; Gembicky, M.; Novozhilova, I. V.; Omary, M. A.; Coppens, P. *Phys. Rev. Lett.* **2005**, *94*, 193003/1–193003/4.
(40) Coppens, P.; Gerlits, O.; Vorontsov, I. I.; Kovalevsky, A. Y.; Chen, Y.; Graber, T.; Gembicky, M.; Novozhilova, I. V. *Chem. Commun.* **2004**, 2144–2145.
(41) Coppens, P.; Vorontsov, I. I.; Graber, T.; Kovalevsky, A. Y.; Chen, Y.; Wu, G.; Gembicky, M.; Novozhilova, I. V. *J. Am. Chem. Soc.* **2004**, *126*, 5980–5981.
(42) Kim, C. D.; Pillet, S.; Wu, G.; Fullagar, W. K.; Coppens, P. *Acta Crystallogr.* **2002**, *A58*, 133–137.

molecules were generated in the crystal by photoirradiation at 29 K. This estimated population of a photoexcited molecule would be somewhat affected by noise density in the photodifference Fourier map (see Supporting Information). But because similar populations in several complexes were obtained by using the least-squares refinement of the response ratio (1.4% and 2.0% in $[Pt_2(pop)_4]^{4-}$ (pop = diphosphonate, $(H_2P_2O_5)^{2-}$), 1.9−2.5% in $[Rh_2(dimen)_4]^{2+}$ (dimen = 1,8-diisocyano-*p*-menthane), 7.3−9.7% in [Cu(dmp)(dppe)]$^+$ (dmp = 2,10-dimethylphenanthroline; dppe = 1,2-bis(diphenylphosphino)ethane)).,[25,40−42] the estimated value should be reasonable.

## Conclusion

In this study, charge transfer from the Au−Cl moiety to the $PPh_3$ ligands in $[AuCl(PPh_3)_2]$ by photoexcitation was directly observed in the novel polymorphic crystal, **1b**, using the photostable X-ray diffraction method. Generation of the charge-transferred state in **1b** was confirmed by comparison with the results of theoretical calculations and measurements of emission spectra. The observed photoexcited structure in **1b** was completely different from that in **1a**, and this is the reason for the difference in emission color between **1a** and **1b** (green and blue, respectively). Comparison of the photoexcited structure and the crystal packing between **1a** and **1b** indicated that the photoexcited structure of $[AuCl(PPh_3)_2]$ depends on the environment surrounding the molecule in the crystal, for example, the molecular arrangement and the reaction cavity. Additionally, integration of the electron density in the photodifference Fourier map and comparison with the results of DFT calculations led to the finding that about 9% of photoexcited molecules were generated in the crystal of **1b** by photoirradiation.

The results of this study also suggest a novel control technique for emission properties in the solid state. The change in the environment surrounding a molecule in the solid state (i.e., making the polymorphic crystal) clearly affected the photoexcited structure and the emission color. This emission-control method, via design of the environment in a solid material, would be a breakthrough in the application of EL materials.

**Acknowledgment.** This work was supported by Grant-in-Aid for JSPS (Japan Society for the Promotion of Science) Fellows. The synchrotron radiation experiments were performed at the BL02B1 at SPring-8 with the approval of the Japan Synchrotron Radiation Research Institute (JASRI) (Proposal No. 2008A1724).

**Supporting Information Available:** Crystallographic information files (CIF) and the PDF containing comments about the population of an excited molecule, all geometrical parameters obtained by X-ray structural analysis, peak wavelengths of every emission spectrum, and Cartesian coordinates for calculated molecules. This material is available free of charge via the Internet at http://pubs.acs.org.